25th Symposium on Naval Hydrodynamics
St. John's, Newfoundland and Labrador, CANADA, 8-13 August 2004

# The use of detached-eddy simulation in ship hydrodynamics

R.J. Pattenden, S.R. Turnock and N.W. Bressloff
(University of Southampton, U.K.)

## Abstract

Accurate numerical simulation of the flow around the hull of a ship remains a challenging task. This work examines whether this is as a result of the inherent unsteady turbulent flow regime influencing the position and strength of vortex systems shed in the wake. To this end the behaviour of the flow around a truncated cylinder is taken as an exemplar of flow at the stern of a ship. Wind tunnel tests of the flow around a KVLCC2 hull form were made to measure the flow field at the propeller plane using particle image velocimetry. Comparison of the instantaneous and the mean flow field indicate significant low frequency effects with large deviations from the mean flow. Such behaviour is also found in the wake of an aspect ratio 1 truncated cylinder. The performance of a detached eddy simulation (DES) approach at capturing the on and off body flow field is compared with detailed experiments and previous calculations of a Reynolds Averaged Navier Stokes with $k$-$\varepsilon$ model and Large Eddy Simulation (LES). The results clearly show significant improvements with the use of DES. Further work is on-going to apply the DES approach to a full ship simulation.

## 1. Introduction

The accurate numerical solution of the flow around the aft end of ship hulls is of interest to naval architects and ship builders. The majority of techniques are currently based on the solution of the Reynolds-Averaged Navier-Stokes (RANS) equations. Closure is provided through the use of a variety of turbulence models of varying degrees of applicability. The solution of steady flow problems, for example when predicting full scale ship resistance, relies on the turbulence model to capture the mean flow behaviour due to unsteady fluctuations in the boundary layer and wake. The RANS approach can give reasonably accurate predictions of the drag and of the mean flow velocities in the propeller plane, but the flow here is a complex shear flow with strong longitudinal vortices created by the curvature of the hull and so it represents a considerable challenge to RANS solvers. This was demonstrated at the Gothenburg 2000 workshop on numerical ship hydrodynamics (Larsson et al., 2000) using the KVLCC2 tanker hullform, developed at the Korean Research Institute of Ship and Ocean Engineering (Van et al., 1998).

Detached-eddy simulation (DES) is a hybrid between Reynolds-averaged Navier-Stokes methods (RANS) and large-eddy simulation (LES), developed by Spalart et al. (1997). It is of interest for high Reynolds number ship flows as it does not require as fine a mesh at the wall as a pure LES approach would, while still working like an LES model away from the wall (ship hull) where the large-scale structures form and convect.

Previous experimental and computational work (Pattenden et al., 2002; Pattenden et al., 2003) has been carried out on a cylinder of diameter/height aspect-ratio 1 mounted on a ground plane. This geometry was used as an exemplar on which to investigate the use of different numerical approaches for three-dimensional separated flows. The flow contains a number of features that are similar to flows around ship sterns, including a large area of attached turbulent boundary layer flow and streamwise vortices.

The objectives of the work presented are threefold:

1. to carry out a wind tunnel study of the flow around a 1:320 scaled model of the KVLCC2 hull form and make instantaneous particle image velocimetry (PIV) measurements of the flow field at the propeller plane;
2. to implement a validated DES method and use it to solve the flow around the truncated cylinder and compare with previous simulations using RANS and LES methods.
3. to prepare for a full DES calculation of the flow around the model scale KVLCC2 hull form.

The paper presents the details of the numerical simulation tool and the implementation of LES and DES used. A description is given of the KVLCC2 wind tunnel tests and results. Results are presented for the DES simulation and comparisons made with experiment and the RANS/LES calculations. Finally

the way forward for full DES calculations of ship forms is proposed.

## 2. Numerical simulation methods

The calculations presented were carried out using a modified version of Elmore (Bressloff, 2001). This uses a finite volume discretisation based on structured multi-block grids using collocated variables. Convective fluxes use the second order, curved line advection method (CLAM) of Van Leer (1974). Diffusive terms use second order central differences. All simulations, including steady RANS are solved as time dependent with a second-order, implicit three time level discretisation.

Appendix 1 gives details of the implementation of the Spalart-Allmaras turbulence model and the LES.

The detached-eddy simulation method was originally proposed by Spalart et al. (1997) as a means of overcoming the considerable computational cost of LES of high Reynolds number flows around real geometries, which is likely to remain prohibitive for many years. It is based on the assumption that RANS models are capable of modelling attached boundary layer flows to a satisfactory degree, so that an LES treatment is only required in the regions of separated flow. As most flows contain large areas of attached flow the computational cost is immediately reduced by using a RANS method in these regions.

The DES method is one of a number of hybrid RANS/LES techniques but is gaining in popularity due to its simplicity. It consists of a modified RANS model which operates as normal close to the walls but switches its behaviour to that of an LES subgrid model away from the walls. This is achieved through the modification of the length scale in the turbulence model, which is related to the distance to the nearest wall for RANS modelling, but changes to be related to the grid spacing away from the wall.

The original DES method was based on the one equation Spalart-Allmaras turbulence model (Spalart and Allmaras, 1994) which uses the distance to the nearest wall as the length scale, $l_{SA}$. For DES this is modified so that it depends on the grid spacing, $\Delta$, as follows,

$$\tilde{l}_{SA} = \min(l_{SA}, C_{DES}\Delta),$$

where $\Delta$ is the largest dimension of the cell, not the cube root of their sum,

$$\Delta = \max(\Delta x, \Delta y, \Delta z).$$

$C_{DES}$ is a constant which defines the transition point between the DES and RANS modes. In isotropic turbulence it has been calibrated to $C_{DES}$=0.65, which has also been found to be valid for most other flows.

The length scale is given as that to the nearest wall boundary. This needs to be calculated once at the start of the calculation on a particular grid as for a multi-block mesh the length scale search process is time consuming in its own right.

The output from an unsteady flow solution at any instant gives a snapshot. However, it is necessary to calculate statistical quantities, which can be achieved by periodically saving the solution and averaging. Unfortunately, for the typically large meshes required for LES or DES calculations the data storage required can become very large. For example, storage of the values of one variable at one time step on a 2.6 million cell mesh requires 12Mb of storage. To minimise the storage requirements a running average approach was used. This was achieved by the addition of statistical variables into the code, which does require more memory but avoids the need to write data to the disk and uses all the available data.

The statistical quantities required for a three dimensional flow are the means of the three velocity components and the components of the Reynolds stress tensor $u_i u_j$. These are defined as follows, for $N$ discrete samples, where $uv$ represents one of the Reynolds stress components.

$$\overline{U} = \frac{1}{N}\sum_{0}^{N} U$$

$$\overline{uv} = \frac{1}{N}\sum_{0}^{N} \left(U - \overline{U}\right)\left(V - \overline{V}\right)$$

It follows that at a time step $n$, $\overline{U}$ and $\overline{uv}$ are given by,

$$\overline{U}_n = \frac{\overline{U}_{n-1}(n-1) + U_n}{n}$$

$$\overline{uv}_n = \frac{\overline{uv}_{n-1}(n-1) + \left(U_n - \overline{U}_n\right)\left(V_n - \overline{V}_n\right)}{n}$$

It is therefore necessary to store nine additional variables, $\overline{U}$, $\overline{V}$, $\overline{W}$, $\overline{uu}$, $\overline{vv}$, $\overline{ww}$, $\overline{uv}$, $\overline{uw}$, $\overline{vw}$. These variables increase the memory requirement by 4%. The values are written to disk along with the all

the other variables for post-processing or to restart the solution.

The largest simulations were run on a minimum of 6 dual-processor nodes (1 GHz Pentium III with 512 Mb of memory). The nodes are connected by 100Mbps Fast Ethernet connections. Typically the truncated cylinder simulations required approximately 1 minute per time-step. This requires one week for 10,000 time-steps. Up to 50,000 time-steps were necessary to obtain converged statistics.

The DNS channel flow solution of Kim *et al.* (1987) was used to demonstrate the performance of the Spalart-Allmaras (S-A) model. In their simulations the Reynolds number based on the mean centreline velocity and the channel half-width, which is equal to the boundary layer thickness, $\delta$, was 3300 ($Re_\tau$=180). The grid size was 192×129×160 in $x$, $y$ and $z$, giving around $4\times10^6$ cells. The dimensions of the domain were $4\pi\delta\times2\delta\times2\pi\delta$ with periodic boundaries in the streamwise and spanwise directions. This size was shown to be sufficient based on two-point correlations.

A two-dimensional grid was used with a length in the $x$-direction of $100\delta$ to allow the boundary layer to fully develop. The number of cells in the streamwise direction was 128. In the $y$-direction the number of cells was varied from 8 to 128 using a non-uniform spacing according to the function (Eisemann, 1979),

$$\frac{y}{L}=\eta p+(1-p)\left(1-\left(\frac{\tanh((1-\eta)q)}{\tanh(q)}\right)\right),$$

where,

$$\eta=\frac{n}{N}$$

Here $n$ is the current node number and $N$ is the total number of nodes on the edge. $L$ is the edge length. In this case $p$=0.064668 and $q$=1.479993 giving a first cell size of $y/\delta$=0.0056 on the finest mesh. This corresponds to $y^+\approx1$. For the purposes of this study the distribution was kept constant so that the wall spacing increased with decreasing grid resolution. The solver was run for 1.5 times the flow-through time.

Figure 1 shows the profiles of velocity and turbulent viscosity, $\nu_t$, at $x/\delta$=100. The flow at this point is fully developed and it can be seen that the agreement with the DNS data of Kim et al. is very good except for the two very coarse grids. The wall cell spacing in the 128×8 and 128×16 grids was

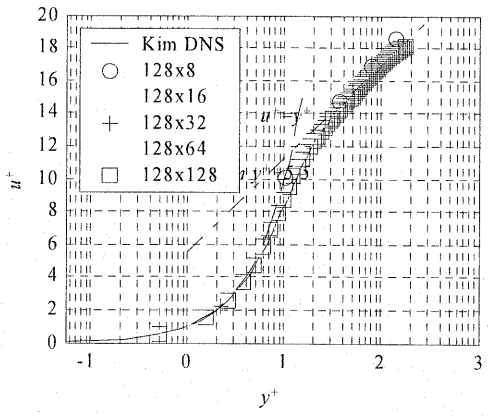


(a) Velocity profile normalised by wall flow

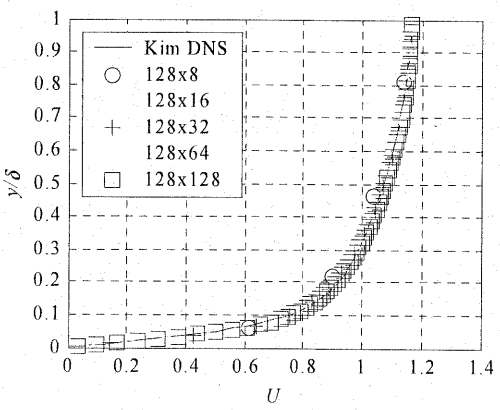


(b) Velocity profile normalised by outer flow

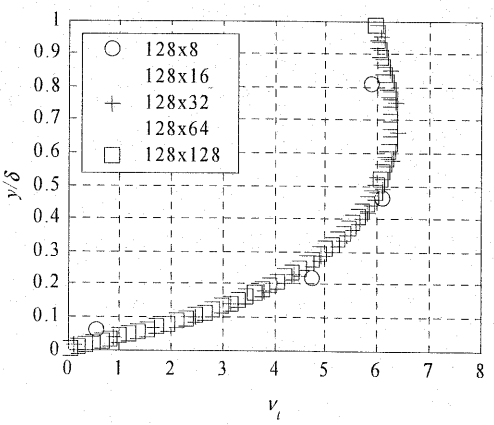


(c) Profile of $\nu_t$

Figure 1: Profiles of velocity $\nu_t$ and for channel flow with different grid resolutions

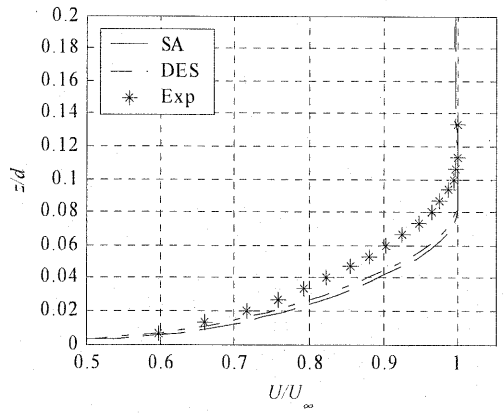


(a) S-A and DES models compared to experiment at $x/d$=-0.5

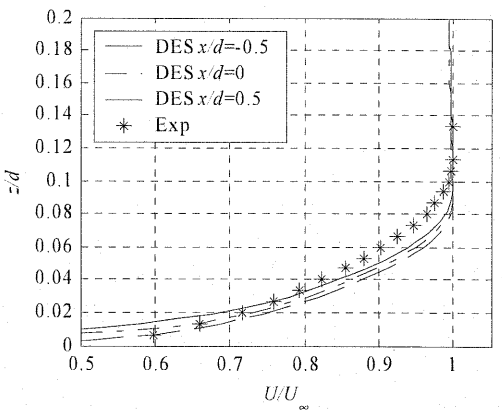


(b) Development of boundary layer using DES through the refined mesh

Figure 2: Results of S-A and DES modelling of turbulent boundary layer

outside the laminar sub-layer and so accuracy would be impaired despite the use of a wall-function.

One of the features of typical DES simulations is that there are regions of boundary layer flows where the along which the grid is refined so that the model will switch from RANS to DES mode. In the case of the truncated cylinder this occurs on the ground plane approaching the cylinder, while on a ship hull the mesh will be refined towards the stern. It is therefore useful to assess the effect of this transition on the prediction of the boundary layer. To do this a simple grid was constructed with the same length and height as the truncated cylinder domain, that is 10.67$d$ long by 4$d$ high. The grid was refined in the $x$-direction at the location of the cylinder. For the RANS cases a two-dimensional grid was used, while for the DES model a three-dimensional grid was employed with a $z$-dimension of 0.05$d$. The grid used is not fine enough to resolve the boundary layer structures properly in LES mode but there is still a region where the grid is refined around the base of the cylinder where the DES mode will be activated. The finest grid had a wall spacing, $y^+$=7, and $x^+$ ranging from 18 to 1080.

The performance of the Spalart-Allmaras RANS and DES models is compared in Figure 2(a). It can be seen that the SA and DES results are very close as would be expected since the DES should be functioning in RANS mode upstream of this point. Figure 2(b) plots the boundary layer profiles of the DES model at different streamwise locations. The first curve at $x/d$=-0.5 is essentially the RANS solution. Beyond this point the grid is refined so that the model operates in LES mode. Here the turbulent viscosity is reduced due to the reduced length scale. If the turbulent fluctuations were simulated correctly in this zone the velocity profile should remain correct. However in this case the profile can be seen to straighten slightly. This suggests that the fluctuations are not being simulated fully. This is likely to be due to the lack of turbulent fluctuations entering this region from the RANS region upstream. This is an acknowledged weakness of DES and applies equally to areas of separation where the separated shear layer does not contain any turbulence from the boundary layer (Travin et al., 2000).

## 3. Wind Tunnel Experiments

The experiments for both the truncated cylinder and KVLCC2 model were carried out in an open circuit suction wind tunnel with a 0.9m wide by 0.6m high and 2.4m long working section. A series of three meshes are used to control turbulence which is measured as 0.3% at the inlet.

Full details of the arrangements for the cylinder tests can be found in Pattenden (2004). The computer simulations were set to reproduce the geometry from the leading edge of the ground plate and include the walls in the same positions. The cylinder has a height and diameter of 150mm. At a speed of 20m/s this corresponds to a Reynolds No. based on diameter of $1.96\times10^5$.

Measurements were made of time varying cylinder surface pressures, surface-flow visualisation using oil evaporation, hot wire anemometry, particle image velocimetry (PIV), and cylinder force measurements.

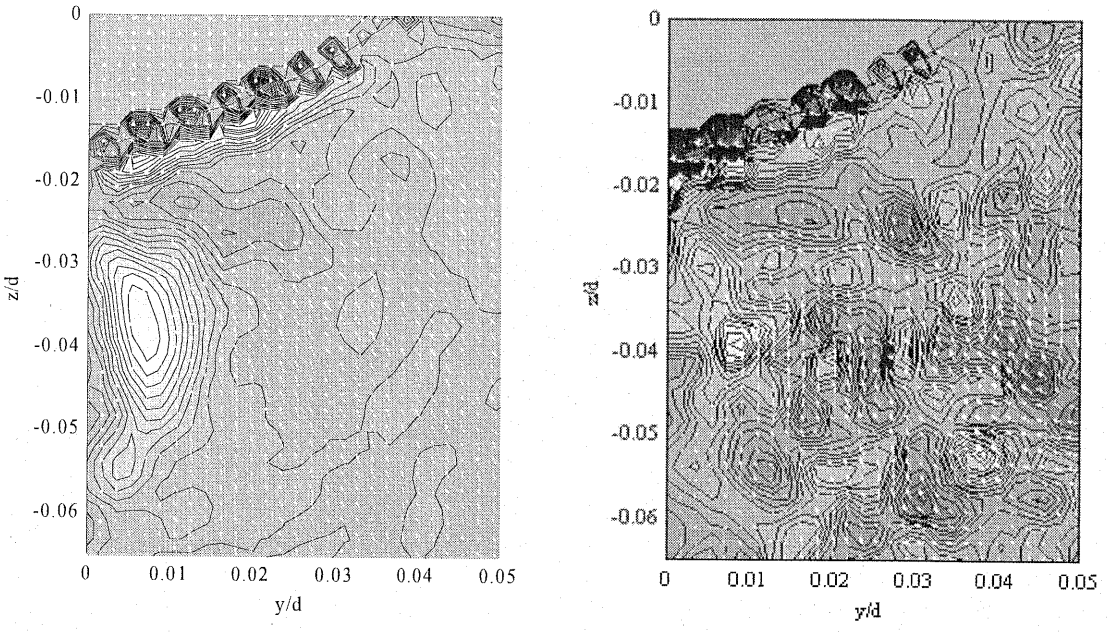


(a) Mean flow

(b) Instantaneous flow

Figure 4: Velocity vectors and vorticity contours of the flow in the propeller plane of the KVLCC2 model

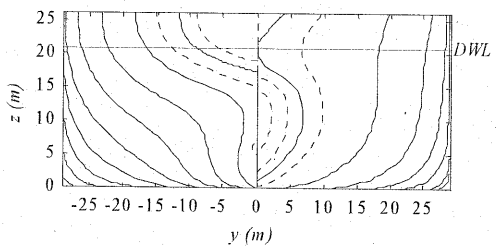


Figure 3: Body plan of KVLCC2 hull

So far only PIV measurements have been made for the KVLCC2 hull model whose body plan is given in Figure 3. A 1/320 scale model (1m long) was commissioned, made of hardwood (Jelutong). The model is divided longitudinally into three sections so that the parallel mid-body can be removed, and also allows for an extra piece to be added above the waterline to increase the depth of the model. The sections are connected with dowel pins. The model was mounted on a ground plate in the wind tunnel in the same way as the cylinder described above. While this is not a strictly accurate representation of the real ship due to the presence of a boundary layer on the ground plate, the CFD model can be set to model this as is the case with the truncated cylinder.

It may also be the case that a double-body model as used in the KRISO tests does not give the same turbulence behaviour as the real ship. This is because the eddies are free to cross the whole wake rather than being constrained by the free-surface.

Particle image velocimetry (PIV) was used to obtain data on the flow in the propeller plane. The laser sheet was oriented in the $y$-$z$ plane so that vectors of $V$ and $W$ were measured. The data was averaged over 500 samples. Only half of the plane was measured to enable greater resolution. The tests were run at a Reynolds number based on hull length of $1.3\times10^6$. The boundary layer on the surface of the hull was tripped using a roughness strip so that the flow is fully turbulent.

Results are presented for the full hull mounted with a depth equal to DWL. Figure 4 shows plots of velocity vectors with contours of vorticity, normalised by the maximum vorticity magnitude.

In the mean flow there are the longitudinal bilge vortices close to the hub of the propeller as found by Van *et al.* (1998). However, as in the truncated cylinder flow these mean vortices appear very unsteady in nature revealing a chaotic instantaneous flow with many large-scale coherent structures. Only in the mean flow do these appear as the two counter-rotating vortices. This is similar to the flow found by Bearman (1997), for the flow

Table 2: Details of truncated cylinder DES results

| *Re* | 100000 | 200000 | 200000 Exp. |
|---|---|---|---|
| CPU time / time step (secs) | 80 | 80 | |
| Side separation, $\phi_s$ (degrees) | 83 | 84 | 70 |
| Primary sep. from ground, $X_{S1}$ ($x/d$) | -1.17 | -1.11 | -1.00 |
| Secondary sep. from ground, $X_{S2}$ ($x/d$) | -0.92 | -0.98 | -0.78 |
| Attachment on free-end, $X_{RT}$ ($x/d$) | 0.47 | 0.41 | 0.17 |
| Attachment on ground downstream, $X_{RF}$ ($x/d$) | 2.2 | 2.1 | 1.6 |
| Local $C_D$ at $z/d$=0.5 | 0.71 | 0.68 | 0.79 |

| | |
|---|---|
| $N_c$ | 324 |
| $N_r$ | 72 |
| $N_h$ | 52 |
| $S_c$ | 0.0098 |
| $S_r$ | 0.002 |
| $S_h$ | 0.002 |
| Total cells | 2,760,960 |

Table 1: Details of DES grid

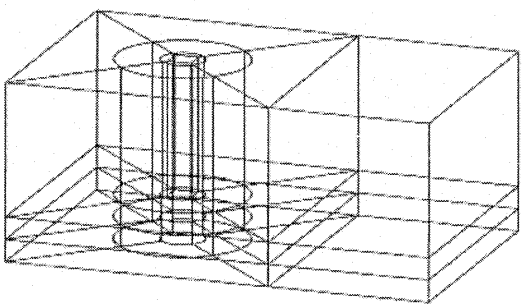

Figure 5: Structure of blocks used to create truncated cylinder mesh

around a car. It is questionable whether the mean flow produced by a RANS calculation or even measured by time-averaging techniques is a valid picture of the flow for many applications. For example the flow over the propeller blades could be more influenced by this short time-scale flow pattern than by the mean flow. While this may not matter for the mean thrust characteristics it may be a factor in the simulation of vibrations and pressure fluctuations.

## 4. Application of DES to a truncated cylinder

Table 1 details the mesh used to solve the DES flow around the truncated cylinder. There were a few minor modifications necessary, (Pattenden, 2004) when compared to the RANS and LES meshes to ensure that the DES solution remained stable. Figure

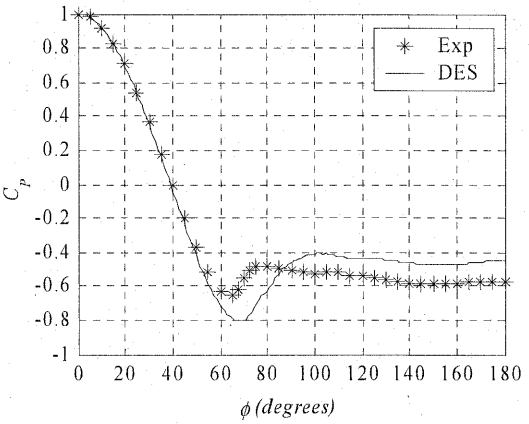


Figure 6: Pressure distribution around cylinder at $z/d$=0.5

5 shows the block structure used. Results are presented for one mesh run at two Reynolds number.

The key parameters characterising the flow field for the two Reynolds numbers are listed in Table 2. The separation from the side of the cylinder occurs at 83 or 84 degrees which is similar to the LES result of 81 degrees. This is also close to the 80 degrees at which the flow separates when the boundary layer is tripped. As the flow in the DES simulation is assumed to be turbulent everywhere it is this value with which the results should be compared.

The extent of the primary horseshoe vortex, defined by the separation point, $X_{S2}$, on the ground plane upstream of the cylinder, is at $x/d$=-1.0 which is further forward than the measured position. This could be due to it being in the ``grey area" between the RANS and DES modes where it has been seen that the boundary layer resolution suffers. It could also be due to weaknesses in the underlying Spalart-Allmaras turbulence model. At the lower Reynolds number the separation point is further forward.

The length of the recirculation region in the wake is characterised by the attachment point on the ground downstream of the body. This is predicted to be $x/d$=2.1 which is exactly the same as the LES and

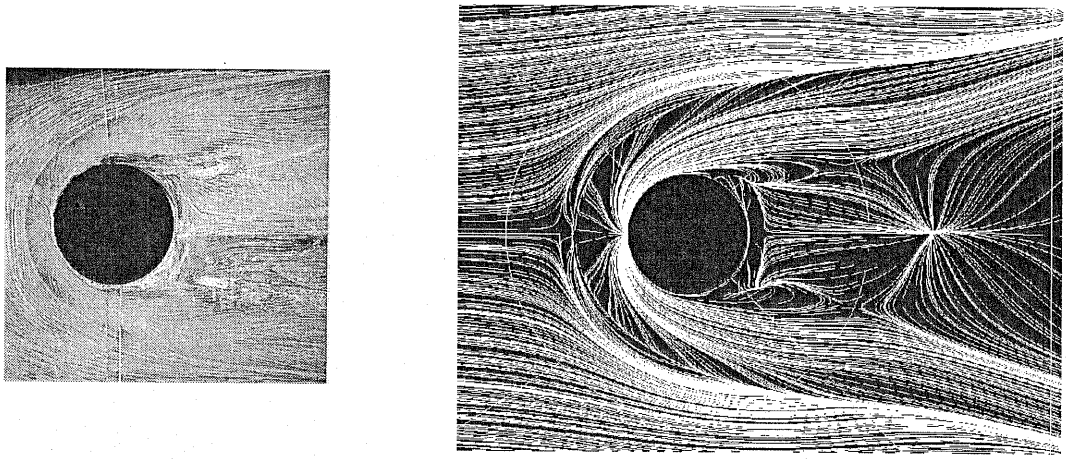

(a) Experiment (b) DES

Figure 7: Surface flow visualisation on ground plane around cylinder

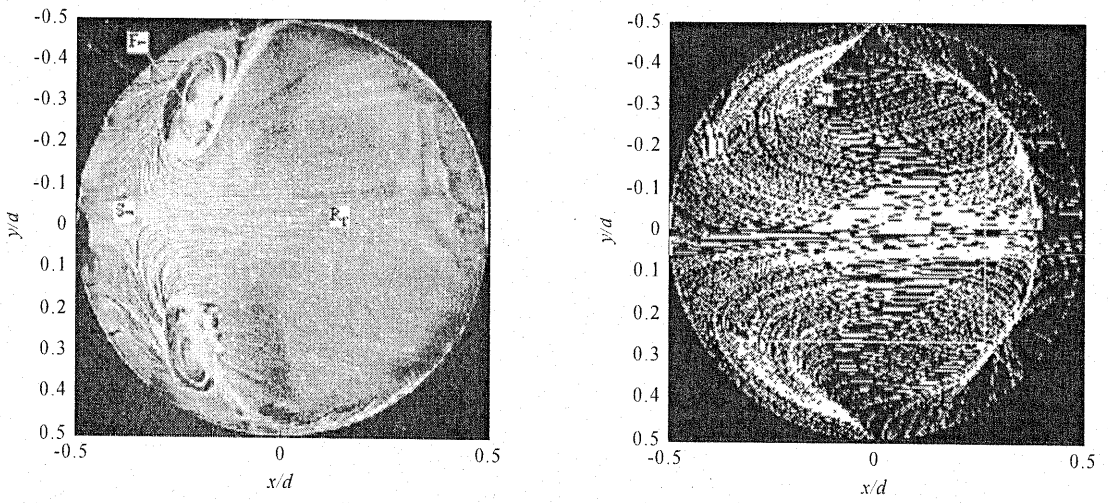


(a) Experiment (b) DES

Figure 8: Surface flow visualisation on free-end of cylinder

$k$-$\varepsilon$ results. This point is slightly further downstream at the lower Reynolds number.

Figure 6 shows the pressure distribution around the cylinder at $z/d$=0.5. The agreement with the experiment is quite good with the slightly later separation and higher base pressure.

One of the motivations for trying the DES technique on this flow was that LES was unable to resolve the boundary layer on the ground plane, which seemed to cause the horseshoe vortex to be incorrectly simulated. The DES method, acting as a RANS model on the boundary layer could be expected to perform as well as the $k$-$\varepsilon$ model at capturing the shape of the primary horseshoe vortex.

In practice however, the DES simulation falls halfway between the LES and $k$-$\varepsilon$ results. As shown by the primary separation position reported above, the horseshoe vortex extends further forward than the one found in the experiment, but not as far as the LES one. In fact the simulations do show a two vortex system as is expected with the primary separation close to the experimental position. The main vortex however is too far upstream with $X_{S2}$=-0.98 compared to $X_{S2}$=0.78. The vortex centre is

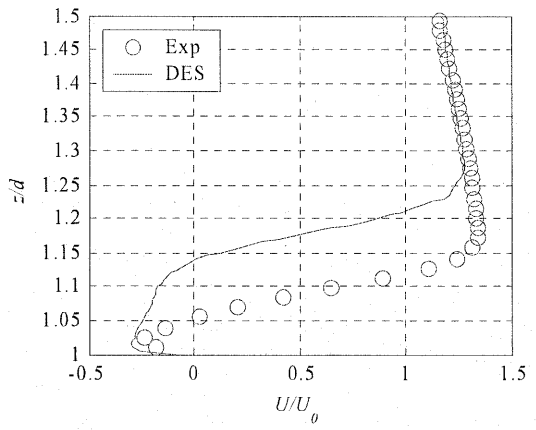


Figure 9: Plot of $U$ against $z/d$ at $x/d$=0 on tip of cylinder

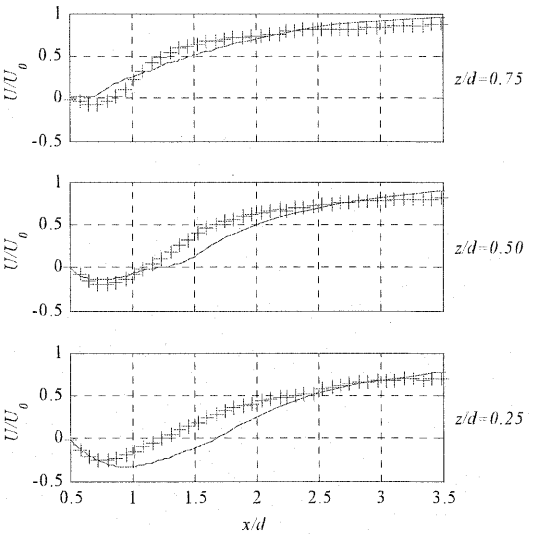


Figure 10: Plot of $U$ against $x/d$ along the centreline in the wake of the cylinder

further forward, and the stagnation point on the cylinder wall appears to be lower than in the PIV measurements. These results are an improvement over both the LES and the $k$-$\varepsilon$ model in terms of the secondary vortices but not as good as the RANS at predicting the primary vortex size and shape. This again may be due to the grey area between the RANS and LES modes of the DES model.

There is also uncertainty over the upstream boundary layer, due to the lack of experimental data with the model in position. Inaccuracies in the approaching boundary layer would affect the formation of the horseshoe vortex. Additional experimental data is therefore needed to be sure about the behaviour of the simulations in this area.

The surface flow patterns in Figure 7 clearly show the separation line at the leading edge of the horseshoe vortex. The flow pattern as the vortex trails downstream shows similar features to the experimental image in terms of the flow directions under the vortex. The differences are caused by the excessive length of the vortex. The separation line on the inside of the horseshoe vortex, marking the edge of the shear layer, diverges at an angle of 17.3 degrees compared to 15.5 degrees in the experimental flow.

The two main aspects which characterise the flow above the free-end of the cylinder are the vertical and streamwise extents of the recirculation bubble and the swirl patterns on the surface of the tip. Figure 8(a) shows the experimental oil flow. The $k$-$\varepsilon$ RANS model completely fails to resolve the detail of the swirls on the tip while the LES reproduces these patterns well. This suggests that the simple no-slip boundary condition with no turbulence model is the best for this swirling boundary layer flow. It might be expected that the DES with its RANS component will damp out some of this motion. The extents of the recirculation bubble on the centreplane are over-predicted by all models so far.

Looking at the surface flow patterns on the free-end, shown in Figure 8(b), as expected the swirl patterns are not completely captured, although the direction of the streamlines is correct. It is just the wrapping up of the vortex eye which is not resolved. The prediction of this flow feature is likely to depend strongly on the ability of the model to predict the boundary layer flow on the top surface of the cylinder. Due to the low speeds and strong pressure gradients in this region the nature of this boundary layer may be difficult to predict using RANS type models.

The vortex on the centre-plane above the cylinder extends too high above the cylinder in the same way as the LES and RANS simulations. Attachment occurs at $x/d$=0.41 which is further back than the experiment. Figure 9, which plots $U$ against $z/d$ at $x/d$=0, confirms that the peak velocity occurs 60% higher than in the experiment. The flow near the surface is faster with a thinner boundary layer. This is where the LES simulation performed well suggesting that the boundary layer prediction with the RANS model is incorrect for this area of the flow.

Figure 10 shows profiles of the $U$ velocity component in the streamwise direction, in the wake of the cylinder. The numerical results can be seen to be close to the experimental values although at the bottom, at $z/d$=0.25, the length of the reversed flow is too long, corresponding to the later attachment on the ground.

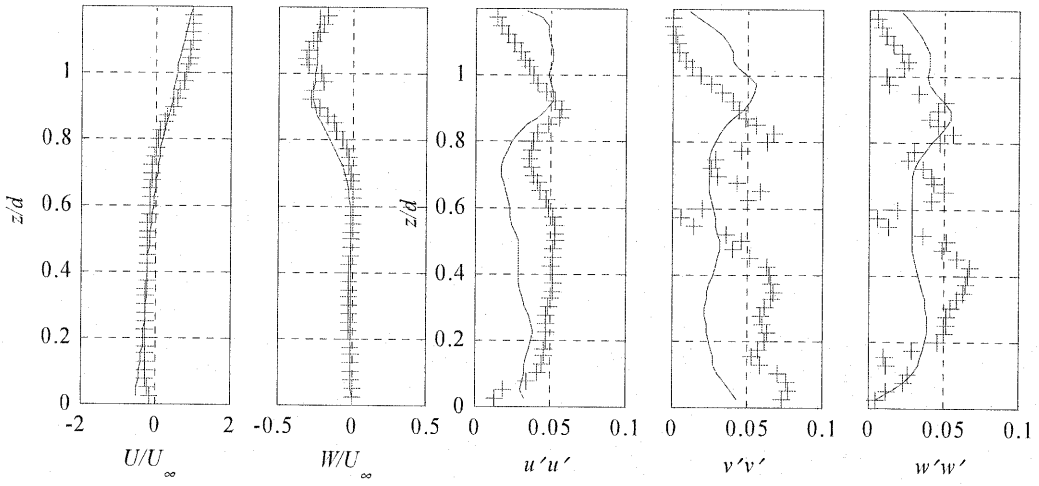


(a) $x/d$=0.83

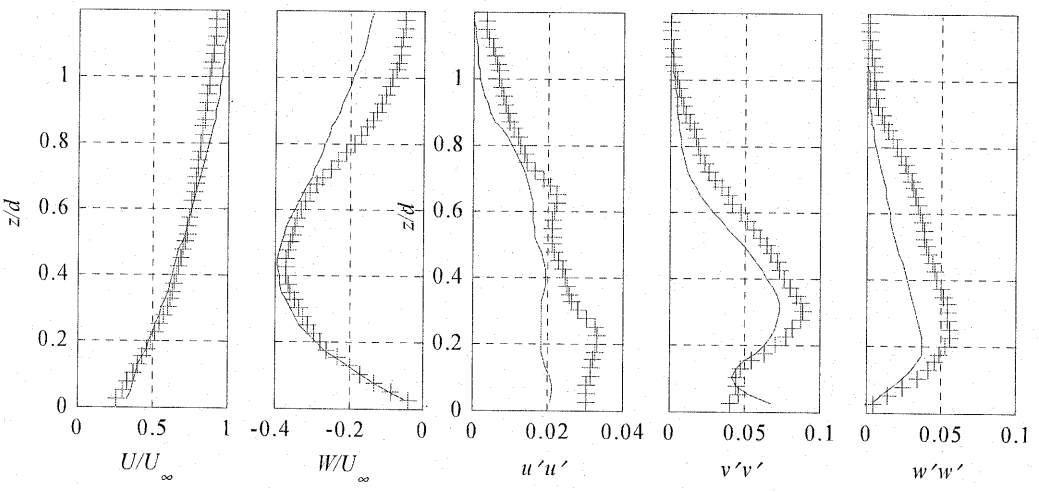


(b) $x/d$=2.5

Figure 11: Profiles of velocity and normal stress components in the wake of the cylinder (+ Experiment, - DES)

Figure 11 shows profiles of velocity components and Reynolds stresses with respect to $z/d$ at various locations in the $x/d$ direction. The profiles of $U$ velocity are quite close to the experimental values except in the shear layer near the cylinder where the peak rise to the free-stream velocity is slower. The later attachment means that the flow near the ground is reversed for longer and is also stronger due to the flatter vortex. The $W$ profiles follow the shape of the experimental curves but the maximum downwash is less due to the shallower angle of the shear layer. The agreement in the lower half of the profiles is quite good. Looking at the normal stresses, $u'u'$ is over-predicted in the shear layer close to the cylinder, as is $w'w'$. $v'v'$ is under-predicted almost everywhere, until after attachment. The difference in the vertical location of the shear layer is evident from the profiles of $u'u'$, which show the peak in the experimental values about $0.2d$ lower in the experiment than in the numerical results at $x/d$=0.83. Although not shown here, the $u'w'$ shear stress agrees quite well with the experimental data with the peaks in the shear layer being very close. In general these profiles show better agreement to the experiment than the LES simulations.

The vector plots in Figure 12 show reasonable agreement particularly downstream where the large streamwise vortices have formed. The tip vortices off the free-end are captured. In the same

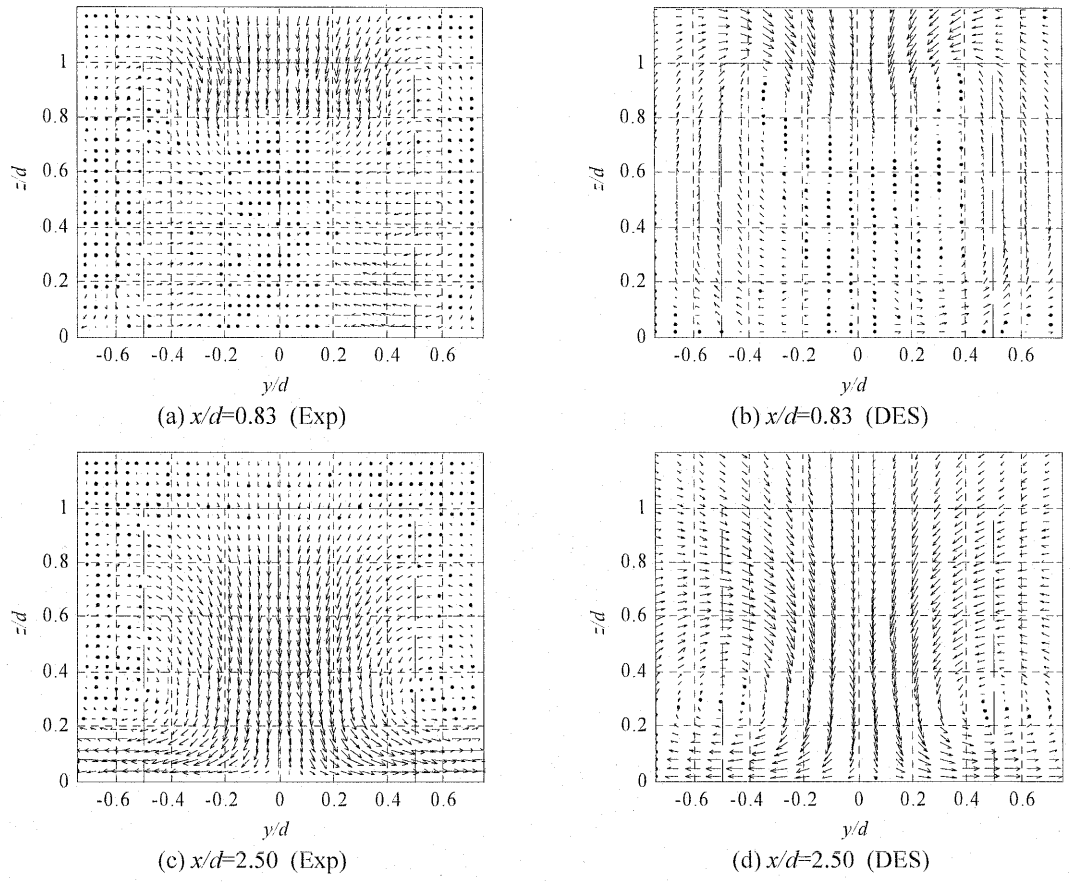


(a) $x/d$=0.83 (Exp) (b) $x/d$=0.83 (DES)

(c) $x/d$=2.50 (Exp) (d) $x/d$=2.50 (DES)

Figure 12: Vector plots of the flow in transverse planes in the wake of the cylinder

way as the previous simulations, the differences can be attributed to the longer recirculation region.

## 5. Why use DES for ship flows?

While many of the features found in the truncated cylinder flow have similarities with the flows found around the sterns of ships, there are certain differences. In particular the Reynolds number around large tankers is typically $10^9$, four orders of magnitude greater than that considered here. There is a long length of attached flow along the hull with a turbulent boundary layer. This boundary layer interacts with the bilge vortex towards the stern to produce a region of unsteady turbulent flow. The turbulent kinetic energy in the propeller plane is lower than that found behind the truncated cylinder $\sqrt{k} = 14\%U_\infty$, compared to $\sqrt{k} = 44\%U_\infty$ but is still large. The other difference is that the transverse normal stresses, $\overline{vv}$ and $\overline{ww}$ are around half of the streamwise stress $\overline{uu}$, whereas in the cylinder wake the streamwise stress is half the transverse stresses. However the flow is still anisotropic and therefore difficult for eddy-viscosity models to predict.

The larger scale structures in the flow in this region are likely to have a characteristic frequency of order 0.01Hz assuming that the non-dimensional frequency is of order 0.1 and that it scales with breadth and ship speed. This corresponds to a period of 100 seconds so the propeller could experience variations in inflow velocity lasting for long periods. It would therefore be useful to be able to simulate this flow as experiments are difficult to achieve at Reynolds numbers anywhere near the full-scale values.

Both the LES and DES results on the truncated cylinder geometry showed that while the agreement between the mean velocity and Reynolds stress profiles was not so good in the recirculating flow close to the cylinder, the results were quite good further downstream, where the flow is dominated by streamwise vortices. It is this part of the flow that probably has most in common with the flow around a ship's stern where the flow undergoes three-

dimensional separation to create streamwise vortices but the dominant flow is still in the streamwise direction.

The main question to be resolved is whether the DES model will behave correctly as the grid is refined towards the stern. It has been seen that there is a grey area in the boundary layer modelling around this interface which can result in an under-resolved boundary layer and high levels of turbulent viscosity being carried into the DES region. DES has been used successfully on a prolate spheroid geometry (Constantinescu et al., 2002) which also has much in common with ship hulls.

As an intermediate step before simulating a full ship geometry, the truncated cylinder grid was stretched in the x-direction to give an elliptical shape with the same length/breadth ratio as the KVLCC2 tanker (Pattenden et al., 2003). The flow in this case is more like the ship flow in that there is no massive separation at the back of the body, but due to the sharp corner at the tip, a pair of longitudinal vortices is formed, equivalent to the bilge vortices. In the mean flow results this pair of longitudinal vortices was clearly visible, but the instantaneous flow is composed of a number of large-scale vortex structures indicating that the longitudinal vortices are unsteady. This again highlights the fact the these longitudinal vortex structures are in fact made up of many smaller chaotic vortices and indicates the need to examine such structures in ship flows as well.

## 6. Conclusions

DES simulations have been performed which show good agreement with the experimental data in predicting flow around a cylinder of aspect ratio 1. In particular the streamwise vortices trailing downstream beyond the region of massive separation are well predicted with the Reynolds stresses agreeing closely with the experimental data.

The quality of the mesh was found to be very important to even get the code to run. In particular attention has to be paid to the cell expansion ratio which should not exceed 1.2.

While the boundary layer upstream was modelled correctly the primary separation from the ground was 22% too far upstream while the secondary separation was 71% too far upstream, resulting in the horseshoe vortex being stretched. This could be due to the switch from RANS to DES mode in the vicinity of the cylinder due to the refined grid. It has been shown that this area poses a problem as the turbulent viscosity due to the RANS/SGS model dies away before the turbulent fluctuations start to develop. Despite this problem the horseshoe vortex is still better than the LES model.

The regions of separated flow, where the DES is functioning as an LES subgrid model, are very close to the LES results. In the wake region the DES appears to give better agreement with the velocity profiles, which could be due to the improved grid used for these computations. The Reynolds stresses though are perhaps slightly worse than the LES ones. The success of the DES simulations on this geometry has indicated that the DES method could be used to simulate the flow around the stern region of full-bodied ships such as tankers and bulk-carriers. Here it should give increased understanding of the nature of the wake flow in the region of the propeller which will be valuable in predicting the performance of the propeller.

Wind tunnel experiments have been carried out at a Reynolds number of $1.3\times10^6$ on a 1m segmented model of the KVLCC2 hullform. The segmented model allows the effect on the stern flow of length and depth to be investigated. PIV measurements have been made of the flow in the stern region, particularly around the propeller plane to investigate the structure of the turbulence here. These show the unsteady nature of the bilge vortex.

It is shown that the cylinder flow has certain features in common with the flow in the propeller plane of the KVLCC2 tanker hull, notably the streamwise vortices, high turbulence intensities and anisotropic stresses.

It is estimated that the energy containing vortices in the wake will have time-scales of the order of 100s which could have an effect on the performance of the propeller and rudder. This is a motivation for the study of the turbulent flow in this region.

## 7. References


Bearman, P. W., "Near wake flows behind two- and three-dimensional bluff bodies," Journal of Wind Engineering and Industrial Aerodynamics, No. 69-71, 1997, pp. 33-54.

Bressloff, N. W., "A parallel pressure implicit splitting of operators algorithm applied to flow at all speeds," Int. Jnl of Numerical Methods in Fluids, Vol. 36, 2001, pp. 497-518.

Constantinescu, G. S., Pasinato, H., Wang, Y.-Q. and Squires, K. D., "Numerical investigation of flow past a prolate spheroid," Aerospace Sciences Meeting, Reno, Nevada, AIAA, 2002.

Eisemann, P. R., "A multi-surface method of co-ordinate generation," Journal of Computational Physics, Vol. 33, 1979, pp. 118-150.

Kim, J., Moin, P. and Moser, R., "Turbulence statistics in fully developed channel flow at low Reynolds number," Journal of Fluid Mechanics, Vol. 177, 1987, pp. 133-166.
Larsson, L., Stern, F. and Bertram, V., Gothenburg 2000: A Workshop on Numerical Ship Hydrodynamics, Gothenburg, Sweden, 2000.
Métais, O. and Lesieur, M., "Spectral large-eddy simulations of isotropic and stably-stratified turbulence," Journal of Fluid Mechanics, Vol. 239, 1992, pp. 157-94.
Pattenden, R. J., Turnock, S. R. and Bressloff, N. W., "An experimental and computational study of three-dimensional unsteady flow features found behind a truncated cylinder," 24th Symposium on Naval Hydrodynamics, Fukuoka, Japan, 2002.
Pattenden, R. J., Turnock, S. R. and Bressloff, N. W., "Developments in the use of large-eddy simulation for ship hydrodynamics," CFD 2003: Computational fluid dynamics technology in ship hydrodynamics, London, U.K., RINA, 2003.
Pattenden, R. J., An investigation of the flow around a truncated cylinder, PhD Thesis. University of Southampton, Southampton, 2004.
Spalart, P. R. and Allmaras, S. R., "A one-equation turbulence model for aerodynamic flows," La Recherche Aérospatiale, Vol. 1, 1994, pp. 5-21.
Spalart, P. R., Jou, W.-H., Strelets, M. and Allmaras, S. R., "Comments on the feasibility of LES for wings, and on a hybrid RANS/LES approach," Advances in DNS/LES, 1st AFOSR Int. Conf. on DNS/LES, Columbus Oh., Greyden Press, 1997.
Travin, A., Shur, M., Strelets, M. and Spalart, P., "Detached-eddy simulations past a circular cylinder," Flow, Turbulence and Combustion, Vol. 63, 2000, pp. 293-313.
Van Leer, B., "Towards the ultimate conservative difference scheme. II. Monotonicity and conservation combined in a second order scheme," Journal of Computational Physics, Vol. 14, 1974, pp. 361-370.
Van, S. H., Kim, W. J., Yim, D. H., Kim, G. T., Lee, C. J. and Eom, J. Y., "Flow Measurement Around a 300K VLCC Model," Proceedings of the Annual Spring Meeting, SNAK, Ulsan, 1998, pp. 185-188.

## 8. Appendix – S-A and LES formulations

### 8.1 Spalart-Allmaras model

The Spalart-Allmaras model (Spalart and Allmaras, 1994) is a one-equation turbulence model developed specifically for external aerodynamic type flows. It is based upon a transport equation for the turbulent kinematic viscosity, $\nu_t$. It contains a destruction term based on the distance to the nearest walls, and an optional trip term to allow laminar to turbulent transition at a specified location. The equations of the model are as follows. A transport equation is solved for $\tilde{\upsilon}$, given by,

$$\tilde{\nu} = \frac{\nu_t}{f_{v1}}, \quad f_{v1} = \frac{\chi^3}{\chi^3 + c_{v1}^3}, \quad \chi = \frac{\tilde{\nu}}{\nu}$$

$$\frac{D\tilde{\nu}}{Dt} = c_{b1}[1 - f_{t2}]\tilde{S}\tilde{\nu} + \frac{1}{\sigma}\left[\nabla\cdot((\nu + \tilde{\nu})\nabla\tilde{\nu}) + c_{b2}(\nabla\tilde{\nu})^2\right] - \left[c_{w1}f_w - \frac{c_{b1}}{\kappa^2}f_{t2}\right]\left[\frac{\tilde{\nu}}{f_{SA}}\right]^2 + f_{t1}\Delta U^2$$

where,

$$\tilde{S} \equiv S + \frac{\tilde{\nu}}{\kappa^2 f_{SA}^2} f_{v2}$$

$$f_{v2} = 1 - \frac{\chi}{1 + \chi f_{v1}}$$

with $S$ being the magnitude of vorticity and $d$ the distance to the nearest wall.

$$f_w = g\left[\frac{1 + c_{w3}^6}{g^6 + c_{w3}^6}\right]^{1/6}$$

$$g = r + c_{w2}\left(r^6 - r\right), r \equiv \frac{\tilde{\nu}}{\tilde{S}\kappa^2 f_{SA}^2}$$

### 8.2 Large-eddy simulation

Large-eddy simulation consists of a time-dependent computation in which the large scale eddies in a turbulent flow are fully resolved, while the smaller scale eddies are modelled. In order to define the equations that are to be solved the flow field must be filtered to remove the smaller scales which are to be

modelled. This operation is typically defined as follows:

$$\bar{U}_i(x) = \int G(x,x')u_i(x')dx'$$

where $G(x,x')$ describes the filter function. In the present studies a box filter is used of width, $\Delta$, equal to the cell size. Any eddies smaller than the filter width are regarded as small eddies and are modelled.

The filtered Navier-Stokes equations are written as:

$$\frac{\partial(\rho\bar{U}_i)}{\partial x_i} = 0$$

$$\frac{\partial(\rho\bar{U}_i)}{\partial t} + \frac{\partial\left(\rho\overline{U_iU_j}\right)}{\partial x_j} = -\frac{\partial\bar{P}}{\partial x_i} + \frac{\partial}{\partial x_j}\left[\mu\left(\frac{\partial\bar{U}_i}{\partial x_j} + \frac{\partial\bar{U}_j}{\partial x_i}\right)\right]$$

The approximation,

$$\tau_{ij}^s = -\rho\left(\overline{U_iU_j} - \bar{U}_i\bar{U}_j\right)$$

is made and is called the subgrid scale Reynolds stress. In most LES methods this stress is approximated by an eddy-viscosity model:

$$\tau_{ij}^s - \frac{1}{3}\tau_{kk}^s\delta_{ij} = \mu_t\left(\frac{\partial\bar{U}_i}{\partial x_j} + \frac{\partial\bar{U}_j}{\partial x_i}\right)$$

There have been many models proposed for the calculation of $\mu_t$ in this equation. The one used in the simulations presented here is the structure-function model as proposed by Métais and Lesieur (1992). Here the eddy viscosity is given by,

$$\mu_t = 0.105\rho C_K^{-3/2}\Delta x F_2^{1/2}$$

where,

$$F_2 = \left(\|\overline{U}(x,t) - \overline{U}(x+r,t)\|^2\right)_{\|r\|=\Delta x}$$

$C_K$ is the Kolmogorov constant and $\Delta x$ is the cell size.